NANO LETTERS
Cite This: Nano Lett. XXXX, XXX, XXX−XXX
Letter
pubs.acs.org/NanoLett

DNA Nanostructures that Self-Heal in Serum

Yi Li[†] and Rebecca Schulman[*,†,‡]

[†]Chemical and Biomolecular Engineering and [‡]Computer Science, Johns Hopkins University, Baltimore, Maryland 21218, United States

Supporting Information

ABSTRACT: Self-assembled DNA nanostructures have potential applications in therapeutics, diagnostics, and synthetic biology. A challenge in using DNA nanostructures in biological environments or cell culture, however, is that they may be degraded by enzymes found in these environments, such as nucleases. Such degradation can be slowed by introducing alternative substrates for nucleases, or by coating nanostructures with membranes or peptides. Here we demonstrate a means by which degradation can be reversed in situ through the repair of nanostructure defects. To demonstrate this effect, we show that degradation rates of DNA nanotubes, micron-scale self-assembled structures, are at least 4-fold lower in the presence of tiles that can repair nanotube defects during the degradation process. Micrographs of nanotubes show that tiles from solution incorporate into nanotubes and that this incorporation increases nanotube lifetime to several days in serum. We use experimental data to formulate a simple model of nanostructure self-healing. This model suggests how introducing even a relatively low rate of repair could allow a nanostructure to survive almost indefinitely because of a dynamic equilibrium between microscale repair and degradation processes. The ability to repair nanostructures could thus allow particular structures or devices to operate for long periods of time and might offer a single means to resist different types of chemical degradation.

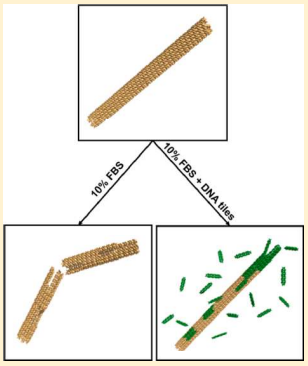

KEYWORDS: *DNA nanotubes, self-assembly, nuclease, self-healing, bionanotechnology*

DNA serves as a powerful and versatile programmable building block for bottom-up-based nanofabrication.[1] For example, DNA nanostructures with precisely defined shapes span three to hundreds of nanometers or even microns.[2−6] Aside from spatial addressability, the mechanical flexibility and biocompatibility mean that DNA nanostructures have a variety of potential applications in diagnostics and therapeutics, especially when these nanostructures are functionalized or serve as a platform for organizing other biomolecules.[7−10]

One of the main challenges to the use of DNA nanostructures in drug delivery and for building biosensors is their rapid degradation in cell culture or in vivo by nucleases, which may be released as dying cells burst or be secreted.[11,12] Fetal bovine serum (FBS), which contains various nuclease enzymes, at 37 °C is commonly used as a model system for understanding how DNA nanostructures might function in in vitro cell culture or in vivo and for characterizing their degradation. Typically, unmodified DNA nanostructures are completely degraded within 24 h when incubated in 10% FBS.[13−16] A variety of approaches have been reported to enhance stability of DNA nanostructures in serum. Cassinelli et al. reported cyclization of DNA strands formed DNA nanostructures with enhanced exonuclease resistance.[16] Coating DNA nanostructures with cationic polymers,[17] lipid bilayers,[18] or oligolysine-PEG polymers[19] has also been reported to shield DNA nanostructures from enzymatic activity. Those reported strategies focused on protecting DNA nanostructures to improve their stability in biological environments. However, chemical modifications or coatings of either DNA strands or nanostructures must be devised specifically to achieve this protection, which for some modifications is labor- or cost-intensive. Modifications to DNA nanostructures, such as the conjugation of DNA to other charged molecules,[17,19] could also compromise the biocompatibility of DNA materials which would be undesirable for some applications.

Here we develop a way to significantly extend the lifetime of a model DNA nanostructure through a self-repair process. When nuclease causes defects in the DNA nanostructure during degradation process, the same monomers that the nanostructure consists of incorporate into the defect sites and replace damaged monomers in the nanostructure. Although DNA nanostructures protected by other approaches would inevitably go through the complete degradation process, the introduced self-repair process induces a repair rate that may fully counteract the degradation rate and thereby has the potential to create a dynamic system in which the DNA nanostructure concentration is maintained for long-term operation. Further, such a process does not depend on chemical modification or coating of the nanostructures and in many cases may work with unmodified DNA, making it potentially compatible with current approaches for large-scale DNA nanostructure synthesis.[20,21]

Received: March 1, 2019
Revised: April 30, 2019

DOI: 10.1021/acs.nanolett.9b00888
Nano Lett. XXXX, XXX, XXX−XXX

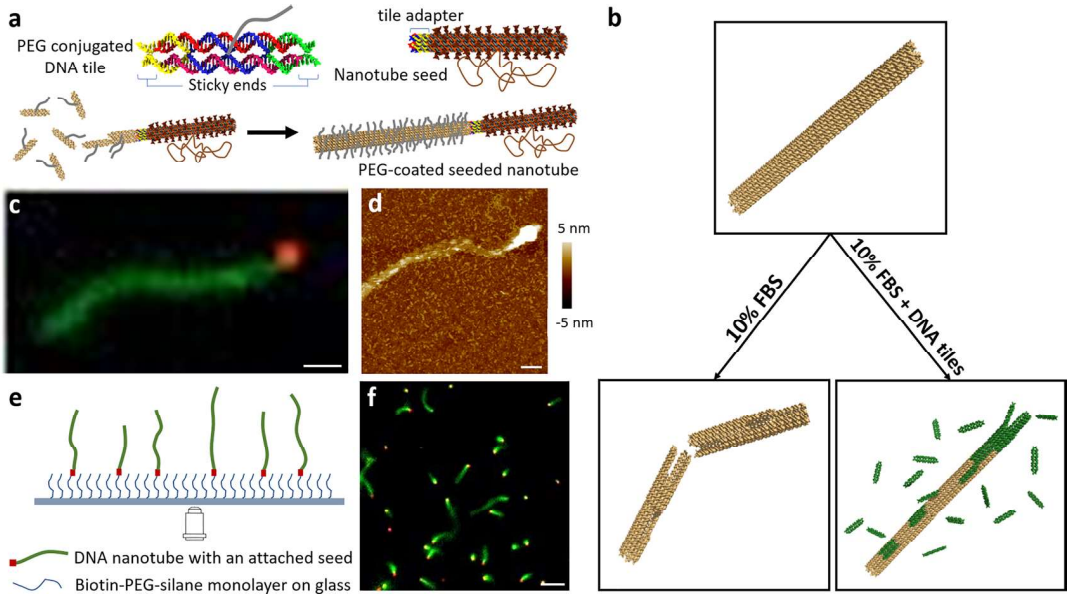

Figure 1. (a) DNA nanotubes self-assemble from DNA tiles via hybridization of complementary single-stranded DNA sticky ends.[27] A DNA origami seed is a thermally stable structure that presents the facet of a growing nanotube using a set of adapter structures that coassemble with the folded DNA origami body of the seed; tile adapters form a domain on one end of the seed that serves as a template for DNA nanotube growth. To prevent DNA nanotubes from sticking to the passivated glass surface in the presence of FBS, one of the strands in the DNA tile is conjugated to a PEG polymer (gray chain). The same DNA strand also has a fluorescent dye to allow visualization of nanotubes via fluorescence microscopy. See Materials and Methods and Supporting Information SI1–SI3 for sequences and synthesis/assembly protocols. (b) Schematic showing the fate of DNA nanotubes in serum-supplemented medium at 37 °C. Although DNA nanotubes degrade rapidly under these conditions, when DNA tiles that make up the DNA nanotubes are also present, these monomers can repair damaged nanotubes, extending nanotube lifetimes. (c) Two-color fluorescence image of a seeded, PEG-modified nanotube. DNA nanotube monomers are labeled with Cy3 dye (green), seed with Atto647 dye (red). Scale bar, 1 μm. (d) Atomic force micrograph of a seeded DNA nanotube with a PEG coating with average width of 24.7 ± 2.8 nm. Scale bar, 50 nm. (e) Schematic showing how nanotubes are anchored by their seeds to a glass surface. To characterize change in nanotube lengths of populations of nanotubes and individual nanotubes over time, seeded nanotubes are anchored to a passivated glass surface through binding of a biotin labeled DNA strand on the seed to NeutrAvidin protein linked to biotin-PEG-silane monolayer on the glass surface (Supporting Information SI4). (f) Multicolor fluorescence image of PEG-coated seeded nanotubes anchored to a passivated glass surface. Scale bar, 5 μm.

We use this self-repair strategy to extend the lifetime of DNA nanotubes in serum. DNA nanotube structures have shown great promise as carriers for drug delivery, due to their high aspect ratio and encapsulation capacity[22,23] and have also been used as components of tissue scaffolds.[24] We demonstrate how DNA nanotubes can overcome damage in serum induced by nuclease degradation through self-repair, specifically, the incorporation of DNA nanotube monomers from solution. Monomers can incorporate within the nanotube body or at nanotube ends, allowing for repair of either lattice defects or decreases in overall nanotube length. This process is modeled after the dynamic assembly and repair of self-assembled structures and cellular architecture observed in living cells that can allow a cell to live for months or years, even though the lifetime of individual proteins ranges from hours to days.[25,26] A simple model that we developed shows how the repair process we demonstrate can lead to increases in nanotube lifetime in serum. This model further suggests how, by properly tuning the dynamics of repair, it should be possible to achieve DNA nanostructure lifetimes of months or longer, much longer than those that might be achieved by relying on the chemical protection of DNA.

DNA Nanotubes Self-Assemble from PEG-Conjugated DNA Tile Monomers. DNA tiles can assemble via Watson–Crick hybridization of their sticky ends to form nanotubes. Seeds are DNA origami structures that present a DNA template that DNA tiles or DNA nanotube ends can attach to via sticky end hybridization. DNA nanotubes were initially formed by isothermal incubation of DNA tile monomers formed from unmodified DNA (Figure S1) with DNA origami seeds[27,28] (Figure 1b) at 37 °C. Nanotubes several microns in length with attached seeds formed during incubation, which we will refer to as seeded nanotubes.

To study the stability of the nanotubes in serum, we incubated the nanotubes in 10% FBS and 12.5 mM magnesium chloride-supplemented Dulbecco's Modified Eagle Medium (DMEM), which we will refer to as serum-supplemented medium, at 37 °C. The supplemented magnesium ions were necessary to maintain the shape of DNA origami structures.[11] We characterized the stability of nanotubes by measuring changes in the two-dimensional (2D) projection lengths of nanotubes over time, after anchoring seeds of seeded nanotubes to the surface of a passivated glass.

We found that aggregation and nonspecific interactions prevented characterization of the anchored nanotubes during incubation. Whereas the PEG monolayer that passivated the glass slide prevented DNA from sticking to the glass surface in standard buffers,[28] in serum-supplemented medium we observed that nanotubes and monomers adhered to the surface over time (Figure S2a). We also observed that DNA nanotubes quickly aggregated when incubated in test tubes with serum-supplemented medium, suggesting that proteins present in cell culture medium could cause undesired hierarchical interactions between nanotubes (Figure S2b).

To prevent these interactions and to make it possible to characterize how the structure of anchored nanotubes changed

DOI: 10.1021/acs.nanolett.9b00888
Nano Lett. XXXX, XXX, XXX–XXX

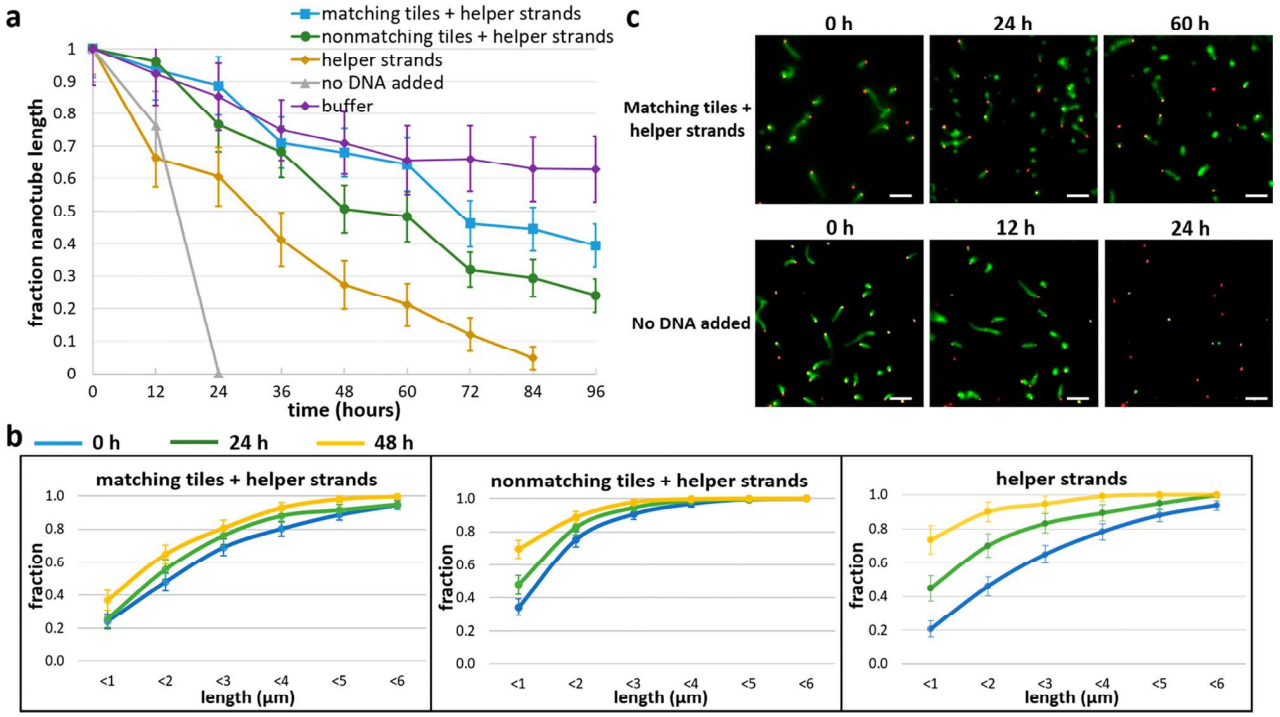

Figure 2. (a) Average nanotube 2D projection lengths after different incubation times at 37 °C in serum-supplemented medium and in TAE Mg^{2+} buffer, normalized as fractions of average nanotube 2D projection lengths before incubation. Error bars are 95% confidence intervals. Helper strands (see text) comprise tile adapter strands (Figure 1) and tile activation strand (Supporting Information SI1). For t = 0, 12, 24, 36, 38, 60, 72, 84, and 96 h, N = 330, 269, 268, 270, 247, 219, 219, 215, and 215, respectively, for the matching tiles + helper strands group; N = 327, 288, 288, 284, 276, 260, 285, 257, and 267, respectively, for nonmatching tiles + helper strands group; N = 309, 185, 161, 132, 111, 92, 67, and 67, respectively, for helper strands group; N = 219, 173, and 152, respectively, for no DNA added group; N = 312, 214, 194, 164, 176, 154, 151, 138, and 128 for buffer group. (b) Cumulative distributions of 2D projection lengths of DNA nanotube at 0, 24, and 48 h. Error bars are 95% confidence intervals. (c) Multicolor fluorescence images of end-anchored seeded nanotubes with a PEG coating at different incubation time points with 267 nM matching tiles and helper strands added and with no DNA added. DNA nanotubes are labeled with Cy3 dye (green), seeds with Atto647 dye (red). Scale bars, 5 μm.

over time in the presence of FBS, we developed a modified type of DNA nanotube by conjugating a 20 kDa molecular weight polyethylene glycol (PEG) polymer to one of the strands of the DNA nanotube monomers (Figure 1a, Figure S3). The position of the conjugation was chosen so that the PEG chain protruded out of the nanotube. Atomic force and fluorescence micrographs confirmed that these modified monomers self-assembled to form nanotubes with attached seeds under the isothermal annealing conditions used to assemble unmodified nanotubes Figure 1c,d). We found that these PEG-coated nanotubes could be anchored to glass surfaces without interacting with the glass surface or aggregating (Figure 1e,f). The PEG-coated nanotubes achieved 2D projection lengths of several microns on average (Figure S8), making it possible to study the breakdown process using fluorescence microscopy.

Breakdown of PEG-Coated DNA Nanotubes in Serum. We first measured the degradation process of PEG-coated seeded nanotubes in serum-supplemented medium at 37 °C by following a population of end-anchored nanotubes over time. The serum-supplemented medium was refreshed every 12 h after images were captured so that enzymes in the serum remained active throughout the experiment. The rate of degradation of the DNA nanotubes was characterized by measuring the 2D projection lengths of the nanotubes at the start of the experiment and at 12-h intervals, and then comparing average length at each time point to the initial average length. When DNA nanotubes were anchored and incubated in serum-supplemented medium at 37 °C, they completely disappeared (i.e., their average length was 0) after 24 h. This rate of degradation is consistent with the observed complete degradation of DNA octahedra,[11] DNA triangular prisms,[15] and DNA tetrahedra[29] in 10% FBS within 24 h. In contrast, PEG-coated seeded nanotubes anchored and incubated in TAE Mg^{2+} buffer at 37 °C, in which buffer was refreshed every 12 h, sustained 85% (±10%) of their initial average 2D projection lengths at 24 h and 63% (±10%) at 96 h. The slow reduction in average nanotube length over time could be a result of melting as monomers can detach from nanotubes at nanotube ends and are not replaced when no free monomers are in the solution.[28] The significantly different rates at which the lengths of PEG-coated DNA nanotubes decreased suggested that although nanotubes could be slowly melted in serum due to the absence of free monomers, enzyme activity in serum played a predominant role in degrading the DNA nanotubes.

DNA Tile Monomer Incorporation Slows down Nanotube Degradation. DAE-E DNA tile nanotubes can assemble through a dynamic process of monomer attachment and detachment.[28,30−32] We hypothesized that a similar dynamic assembly process could counteract degradation by allowing monomers to incorporate at the sites of enzyme-induced defects as well as at nanotube ends. In such a case,

DOI: 10.1021/acs.nanolett.9b00888
Nano Lett. XXXX, XXX, XXX−XXX

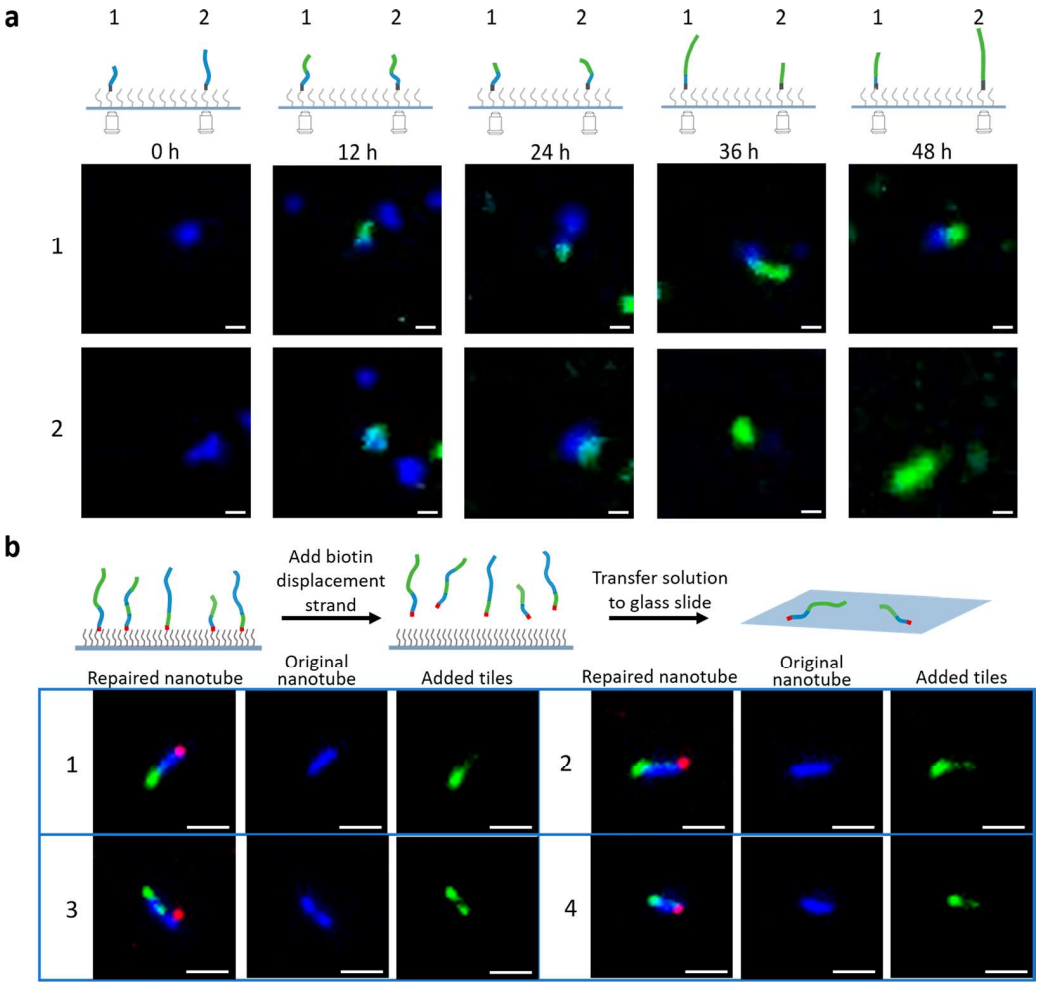

Figure 3. (a) Multicolor confocal micrographs and corresponding schematics of two example-anchored DNA nanotubes (blue, Atto488) before and at different time points during incubation with free nanotube monomers (green, Cy3) in serum-supplemented medium. The free monomers can both incorporate within nanotubes and extend existing nanotubes. Seeds are not shown. Scale bars, 2 μm. (b) Four sets of multicolor fluorescence micrographs showing nanotubes that were incubated in serum-supplemented medium for 24 h while anchored by their seeds to a glass-bottomed dish. After incubation, the anchor was detached from the surface using a strand displacement process (Supporting Information SI4.2) and the solution containing the detached nanotubes was deposited onto glass slides for fluorescence imaging, as illustrated in the schematic. Images of repaired nanotube are overlays of the images from the channels used to measure the original nanotubes (monomers were labeled with Atto488), free monomers present in the incubation solution (Cy3), and the seed (Atto647). Scale bars, 2 μm.

freely diffusing DNA tiles in solution could repair the structures by replacing damaged tiles in the nanotubes.

To determine whether such a repair process might be feasible, we first asked whether free monomers might be able to incorporate within an existing nanotube as well as at nanotube ends. We grew DNA nanotubes from monomers labeled with one fluorescent dye and then incubated them with monomer tiles labeled with a second dye so that incorporation after growth in TAE Mg^{2+} buffer could be visualized (Supporting Information SI10). Monomers with the second dye were annealed in inactive form to prevent their assembly, and a DNA strand to activate tiles was added when the tiles with the second dye were added to the assembled nanotubes labeled with the first dye (Materials and Methods, Supporting Information SI1.3, 3, 11). We found that for some combinations of dyes, monomers were incorporated within nanotubes in addition to at nanotube ends (Figure SI13), suggesting that monomer incorporation could occur at sites within nanotubes.

We next studied the effects of additional free monomers on the lifetime of PEG-coated DNA nanotubes in serum-supplemented medium by adding annealed DNA tiles in an inactive form into the solution to a final concentration of 267 nM at the start of the experiment. A DNA strand, which we called activation strand, was then added to the mixture to transform the added tiles into an active form. To ensure that the tiles in solution could bind to the seeds and that nanotubes would not become irreversibly attached from seeds, we added adapter strands (which form the seed's interface to the tiles) to the mixture along the activation strand (Supporting Information SI1). We referred to the activation strands and adapter strands that were added to the solution collectively as helper strands. The medium and new tiles were refreshed every 12 h. Under these conditions, the lifetime of nanotubes was dramatically longer than the lifetime of nanotubes incubated in serum without additional DNA; nanotubes incubated with tiles and helper strands were 40% ($\pm$7%) as long after 96 h as they were at the start of experiment, whereas nanotubes incubated without tiles or helper strands had degraded completely by 24

DOI: 10.1021/acs.nanolett.9b00888
Nano Lett. XXXX, XXX, XXX−XXX

h (Figure 2a). Until the incubation time of 60 h, the DNA nanotubes in "matching tiles + helper strands" group had statistically indistinguishable fractional average lengths as the DNA nanotubes in "buffer" group had, suggesting the repair of nanotubes by free tiles in serum could fully counteract the degradation of nanotubes by enzymes for over 2 days. In addition, although the degradation of nanotubes without DNA being added occurred precipitously, the decay of nanotubes in the presence of tiles and helper strands was gradual; the distribution of nanotube lengths measured changed only slowly over time.

The DNA added to the solution that the nanotubes were incubated in could have decreased the rate of nanotube degradation either by repairing the nanotubes or by serving as a competing substrate for nuclease degradation, thereby slowing down the rate of nanotube degradation. To verify that the replacement of damaged monomers by undamaged monomers was important for extending the lifetime of nanotubes in serum, we next tested how adding different types of DNA to the surrounding solution changed nanotube degradation rates. Adding only the helper strands resulted in longer nanotube lifetimes than adding no DNA at all, but the lifetimes of nanotubes were significantly shorter than the lifetimes when tiles were also included; the majority of nanotubes were less than 1 μm in length after 48 h (versus fewer than 25% at the start of the experiment) (Figure 2b) and more than 90% of the nanotubes' total length was lost after 84 h of incubation (Figure 2a). However, in this case the total concentration of DNA in solution was less than the total amount of DNA present in the solution of helper strands and tiles during the experiments testing repair. To test the extent to which this lower total DNA concentration in solution was a factor in the decreased nanotube lifetime, we next characterized nanotube lifetime in a solution containing the same total concentration of DNA as the nanotube tiles and helper strands solution, but we replaced the DAE-E nanotube tiles with DAE-E tiles with sticky-end sequences that were not complementary to the sticky ends on the nanotubes. The noncomplementary sticky-end sequences prevented these tiles from incorporating into the nanotubes. We called these tiles nonmatching tiles. Nanotubes incubated in the solution of helper strands and nonmatching tiles also had shorter lifetimes and a greater reduction in average nanotube length than nanotubes incubated in a solution of helper strands and tiles that could incorporate into nanotubes. In addition, when both helper strands and nonmatching tiles are present, nanotubes had longer lifetime compared to nanotubes incubated in only helper strands, suggesting that increasing the amount of added DNA also slows degradation by serving as competing substrates to nuclease.

Incorporation of DNA Tiles into Nanotubes during Degradation. The observation that the presence of matching tiles increased nanotube lifetime more than the presence of nonmatching tiles at the same concentration suggested that the incorporation of tiles into nanotubes could increase their lifetime in serum. We thus next sought to determine whether matching tiles incorporated into nanotubes during the degradation process. To make it possible to visualize the incorporation of tiles during degradation, we prepared nanotubes assembled from tiles labeled with one dye (Atto488) and incubated these nanotubes in serum-supplemented medium containing matching tiles labeled with a different dye (Cy3). This pair of dyes was chosen to allow simultaneous imaging of the original nanotubes and added tiles using a dual-camera on a spinning disk confocal microscope that could simultaneously capture images of the two types of tiles within individual nanotubes during the growth process. Comparisons of images of the same anchored nanotubes after different incubation times showed how the matching tiles could extend nanotubes and that matching tiles could incorporate into the bodies of existing nanotubes (Figure 3a). In some cases the nanotubes anchored to the surface eventually consisted entirely of the matching tiles that were in the incubation solution (Figure 3a, nanotube 2).

Whereas simultaneous two-color imaging made it possible to follow the degradation and recovery of a single nanotube over time, it was in general difficult to determine how nanotube tiles incorporated within a nanotube using this technique because many parts of the nanotube, which could move in three-dimensions, were not in sharp focus. To better visualize how matching tiles became incorporated into nanotubes during degradation, we anchored nanotubes to a glass bottom dish with a DNA linker that could be detached using a DNA strand displacement process (Supporting Information SI4.2). We incubated nanotubes with this linker on dishes in serum-supplemented medium at 37 °C for 24 h in the presence of Cy3-labeled matching tiles; the solution was replaced with fresh medium and tiles at t = 12 h following our previous experiments. The nanotubes were then detached from a dish by adding the displacement strand, and the resulting solution was plated on microscope slides (see Materials and Methods). Images of these nanotubes showed that tiles incorporated not only at the ends of nanotubes but also within the original nanotubes (Figure 3b). The incorporation of tiles in small regions of the original nanotubes suggesting that the matching DNA tiles in solution could repair damaged DNA nanotubes.

A Model of the Dynamics of DNA Nanotube Degradation and Repair. Our observations of matching tile incorporation into nanotubes during degradation demonstrated that tiles incorporated into and extended nanotubes when longer nanotube lifetimes were observed. To understand how and the extent to which the incorporation of DNA tiles or other DNA species might affect the kinetics of nanotube degradation in the presence of nucleases, we created a simple model of nanotube degradation and repair. To focus on the role of repair rather than nanotube regrowth, the model included only incorporation of tiles into an existing nanotube and ignored the possibility of nanotube growth.

The model represents the nanotube as a cylindrical lattice of monomers connected according to the connectivity imposed by nanotube sticky ends. Nanotubes were assumed to be six monomers in circumference, in accordance with previous measurements of the circumference of seeded DNA tile nanotubes.[27,30] Within the model, a nanotube initially starts out at a particular length; the number of rows was chosen assuming that if monomers are 14.3 nm long,[30] each row of monomers contributes the same to total nanotube length. Nucleases were assumed to degrade nanotubes by removing individual tile monomers at a given stochastic (microscopic) reaction rate. Although the removal of a small number of monomers would create holes in that lattice but leave it connected, the removal of too many would cause the nanotube to sever. In our simulation, we assumed that severing would occur when the lattice of tiles that formed the nanotube became disconnected, forming two nanotubes that start and end respectively at the point at which the discontinuity arose.

DOI: 10.1021/acs.nanolett.9b00888
Nano Lett. XXXX, XXX, XXX−XXX

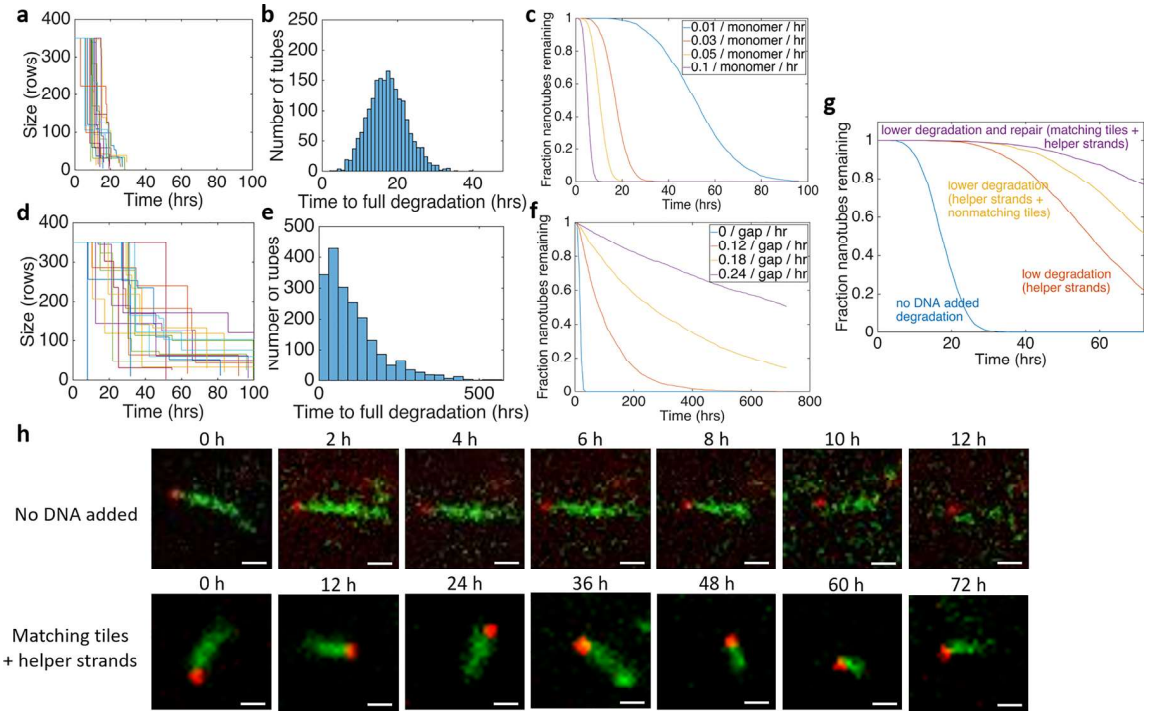

Figure 4. Simulated nanotube degradation and repair and differences in the dynamics of nanotube degradation and nanotube coupled degradation and repair observed in experiments. (a) Example lengths of nanotubes over time predicted by a stochastic kinetic model of nanotube degradation in which individual monomers are removed from the nanotube at a rate of 0.03/monomer/h. (b) Distribution of times at which individual simulated nanotubes became short enough to be considered degraded. (c) Fractions of nanotubes remaining in simulation over time for different monomer degradation rates. (d–f) Simulations and results as in (a–c) except that monomers can be degraded and gap sites in the lattice neighboring at least two intact monomers can be repaired by the incorporation of a tile from solution. The repair rate is 0.12/gap/h in (d,e) and as shown in (f). (g) Predicted fractions of nanotubes remaining over time made using simulations from (a–f) to compare with the results of experiments made by choosing appropriate degradation and repair rates; for experiments with baseline degradation or no DNA added (0.03/monomer/h), reduced rates of degradation that would be expected for when helper strands (0.009/monomer/h) and helper strands and monomers with unrelated sequences (0.007/monomer/h) were added to the buffer and when nanotubes were both being degraded (0.007/monomer/h) and repaired (0.009/gap/h) when helper strands and matching tiles were present in buffer. (h) Time-lapse multicolor fluorescence micrographs showing seeded nanotubes incubated in serum-supplemented medium at 37 °C. When no DNA was added, the DNA nanotube remained intact for a few hours before rapidly disassembling. When 267 nM matching tiles were present in solution, refreshed every 12 h, a typical DNA nanotube was not completely degraded over several days but decreased gradually in length. Scale bars, 1 μm.

To directly compare the model's results to our experiments, we simulated the reactions of tile degradation by cleavage in a stochastic kinetic simulation (see Materials and Methods) and tracked how the lengths of anchored nanotubes changed over time. (The dynamics of the nanotube fragments that became disconnected from the anchored structures were not simulated after their disconnection.) During the simulated degradation of a population of nanotubes that were initially 5 μm long, nanotubes remained at their initial length for some period of time but then suddenly severed. After an initial severing event, a nanotube rapidly severed again and again until it was short enough to be considered fully degraded (Figure 4a). This type of relatively sudden decrease in nanotube length was observed in experiments where DNA was not added to the serum during incubation (Figure 4h and SI Movie 1, Figure S17).

The distribution of nanotube severing times in serum without additional DNA present predicted in the model was qualitatively different than the distribution of times of degradation of individual tiles. Tile degradation events should be broadly (i.e., exponentially) distributed, following the memoryless nature of the degradation reaction. In contrast, severing events were tightly clustered in a peaked distribution, presumably because severing happens when the fraction of defects in the tube approaches the critical fraction where the nanotube's lattice would no longer be connected.

To compare the predictions of the model with our experiments, we assumed that a nanotube would be considered degraded in micrographs when it became too short to be seen clearly, about 30 rows of monomers in length. The distribution of times at which a 5 μm long tube reached this state in simulations of nanotube degradation are shown in Figure 4b. These decay times are clustered in a peaked distribution. Changing the rate of decay, as might occur with the introduction of a competitor species for nucleases, such as the helper strands or tiles with random sequences, would be expected to slow degradation. Simulations suggest that slowing the rate of degradation would shift the average time at which degradation occurred but would still cause most nanotubes to persist and then degrade within a relatively short period (Figure 4c).

Qualitatively different behavior was observed in simulations where both degradation of monomers and lattice repair, modeled as reincorporation of an intact tile at a site where a tile had left, was allowed. Instead of nanotube severing events being clustered in a narrow range of time, nanotubes could sever and then persist for a long time before severing again (Figure 4d). The resulting times at which nanotubes reached

DOI: 10.1021/acs.nanolett.9b00888
Nano Lett. XXXX, XXX, XXX−XXX

the fully degraded states were thus spread across a distribution with a long tail (Figure 4e), in contrast to the distribution of times that was clustered around a particular peak time observed when nanotube monomers could be degraded and repair could not occur (Figure 4b). Repair thus allows some nanotubes to persist for very long times even when on average nanotubes still decay quickly. Our simulations also predict that increasing the repair rate could allow most nanotubes to last for very long times.

While decreasing the monomer defect rate effectively delays the time to full degradation by a linear factor, increasing the repair rate slows the rate of degradation much more rapidly and extends the range of lifetimes by introducing a long tail to the lifetime distribution (Figure 4f). These qualitative changes in the distribution of nanotube lifetimes persist in a simulation of nanotubes with the same distribution of initial lengths as those used in this the time-lapse degradation experiments (Figure S12).

A degradation process in its simplest form might be viewed by analogy to a Poisson process, in that decreasing the effective rate of repair increases the expected time before a certain number of defects arise by a linear factor. In contrast, a degradation process in which repair was faster on average than degradation might be viewed as a reverse-biased random walk, such that the expected time to sever at a particular point is on order exponential in the number of monomers that must be degraded in a local region of the nanotube lattice to cause severing. Increasing the ratio of the monomer repair rate to monomer degradation rate has the effect of increasing the base of this exponent. Because the number of monomers that must be degraded in the nanotubes we have studied is large (on order 6), the inclusion of repair dramatically affects how the lifetime of a structure can be manipulated. For example, simulations predict that increasing the repair rate by just a factor of 2 for a process that allows the majority of nanotubes to survive for 2−3 days could allow the majority of nanotubes to survive for more than a month (Figure 4f). Thus, the use of repair could be an important strategy for structures and devices that are designed to persist for months or years in an environment where degradation of components is likely to occur.

In this paper, we report a dynamic DNA nanotube system that allows the degradation of DNA nanostructures in serum to be reversed through in situ self-repair. While PEG-coated DNA nanotubes, self-assembled from monomers, were completely degraded after 24 h incubation in serum-supplemented medium at 37 °C, their lifetimes were significantly increased when free monomers were introduced in the solution. Free monomers repaired the degrading nanotubes by replacing damaged monomers that made up the nanotubes and joining onto nanotube ends. The increase in nanotube lifetime was enhanced by the fact that monomers can serve as a competitor to DNA nanotube as enzyme substrates. We developed a stochastic kinetic model to simulate the dynamics of nanotube degradation and repair. The predictions of this modelmatched our experimental results and showed how inclusion of repair rate in a degrading system could allow nanostructures to persist for a long time.

Another important challenge to using DNA nanostructures for in vivo applications is that the high concentration of magnesium ions needed to stabilize DNA may be incompatible to in vivo systems.[33] Approaches developed by other investigations might help stabilize DNA origami in physiological conditions. For instance, Shih et al. reported oligolysine-PEG conjugate coating prevents DNA origami structures from low-salt denaturation.[19] Cassinelli et al. reported using click chemistry to form DNA catenanes allow nanostructures to remain stable without salts.[16] Tuukkanen et al. reported DNA nanostructures deposited through a spray-coating method are stable in salt-free solution.[34] Those reported approaches may be used in tandem with our approach of increasing nanostructure lifetime in serum to advance the potential of DNA nanostructures for use in vivo applications or other environments where degradation of DNA occurs.

Materials and Methods. *Materials.* Tris/acetate/EDTA (TAE) buffer was purchased from ThermoFisher Scientific. Dulbecco's Modified Eagle's Medium (DMEM), magnesium acetate tetrahydrate, nickel(II) sulfate, tris-HCl, sodium chloride, and Tween-20 were purchased from Sigma-Aldrich. Fetal bovine serum (FBS) was purchased from Gibco. Polymer succinimidyl valeric acid PEG_{20k} (PG1-SVA-20k) was purchased from NANOCS. Amicon ultrafiltration device was purchased from Fisher Scientific. Glass bottom dishes with 50 μm grids (81148) were purchased from ibidi.

Conjugation of PEG to DNA Tiles. The central strand of each DNA tile had a 5′ Cy3 or Atto488 fluorescent dye modification for fluorescence imaging of nanotubes and a 3′ primary amine modification for covalent conjugation with PEG_{20k}-SVA (Supporting Information SI1). The DNA strand and PEG_{20k}-SVA were conjugated by preparing a mixture of 50 μM of the DNA strand and 2 mM PEG_{20k}-SVA in PBS buffer. The mixture was agitated overnight at room temperature. The DNA-PEG_{20k} conjugate was then PAGE gel-purified. The concentration of purified conjugate was determined by comparing the fluorescence of conjugates against the fluorescence of a ladder of concentrations of fluorescent central strand of DNA tile using a MX3005P qPCR System (Agilent).

Assembly of Seeded Nanotubes To Be Anchored to Glass. The 7,240bp M13mp18 scaffold strand was purchased from Bayou Biolabs. All other DNA was purchased from Integrated DNA Technologies, Inc. Nanotube seeds and inactive DNA tiles were prepared and annealed separately. The nanotube seed assembly mixture consisted of 5 nM scaffold strand, 200 nM staple strand mix, 100 nM adapter mix, 25 nM attachment strand mix, and 300 nM biotin linker strand mix (Supporting information SI4). Inactive DNA tiles were prepared by mixing the six inactive tile strands (sequences, Supporting information SI1.3) including PEG_{20k} conjugated central tile strand, each at 350 nM concentration. All mixtures were prepared in TAE Mg^{2+} buffer (40 mM Tris-Acetate, 1 mM EDTA) with 12.5 mM magnesium acetate added.

Both seed and inactive tile assembly mixtures were subjected to a thermal annealing ramp with an Eppendorf Mastercycler according to the following program: incubate at 90 °C for 5 min, decrease to 45 °C at 1 °C/min, incubate at 45 °C for 1 h to allow formation of seed origami and inactive tiles, and decrease to 37 °C at 0.1 °C/min.

After annealing, nanotube seeds were separated from excess staple strands using a 100k MWCO Amicon Ultra centrifugal filter device (Millipore). Following purification, 10 μL of 1μM Atto647-modified DNA strand was added to 40 μL purified nanotube seed sample and incubated at room temperature for 15 min to allow fluorescent labeling of seeds. The concentration of fluorescently labeled seeds was set to 1.6

DOI: 10.1021/acs.nanolett.9b00888
Nano Lett. XXXX, XXX, XXX−XXX

nM, determined by measuring the concentration of a stock solution by counting the number of seeds per field of view (86 μm × 86 μm) after imaging them on a glass slide with fluorescence microscope (Olympus IX71) and then diluting this solution appropriately. A total of 1.8 μL of these fluorescently labeled seeds and 0.8 μL of tile activation strand (10 μM) were then added to 17.4 μL of the annealed tile sample. The sample was incubated at 37 °C for at least 15 h for nanotubes to grow.

Glass Surface Treatment and Attachment of Seeds to Glass. For all time-lapse experiments, seeded nanotubes were anchored via biotin-NeutrAvidin linker chemistry to passivated 0.17 mm-thick glass. The glass was passivated by attaching a biotin-labeled PEG-silane monolayer (Supporting Information SI4), after which NeutrAvidin protein (ThermoFisher Scientific 31000) was then added. A biotinylated DNA "universal biotin attachment strand" was then added to the passivated glass and incubated at room temperature for 15 min. The surface was then washed with TAE Mg^{2+} buffer three times. Seeded nanotubes with six linker strands complementary to the universal biotin attachment strand were then added into the dish and incubated at room temperature for 10 min. The glass was then washed with TAE Mg^{2+} buffer three times to wash away unanchored nanotubes before starting the experiment. In experiments in which DNA nanotubes were detached from the dish, an extended universal biotin attachment strand with a 5′ toehold domain not complementary to the linker strand was used to allow liftoff of seeded nanotubes by adding a displacement strand fully complementary to the extended universal biotin attachment strands (Supporting Information S4.2).

Fluorescence Microscopy. For time-lapse experiments in which nanotubes were characterized at 12 h intervals, nanotubes anchored on glass were washed before each imaging step to reduce background fluorescence by pipetting 400 μL TAE Mg^{2+} buffer onto the dish and removing it three times.

In wide-field fluorescence microscope experiments, samples were imaged on an inverted microscope (Olympus IX71) using a 60×/1.45 NA oil immersion objective lens. At the initial time point, four locations indicated by the grid markings printed on the dish under bright field were identified to allow imaging of the same locations at subsequent time points. To estimate nanotube lengths, one image of seeds and five images of nanotubes were captured at each location.

For confocal fluorescence microscope experiments, samples were imaged on an inverted microscope with a spinning disk unit (Zeiss AxioObserver Yokogawa CSU-X1M Spinning Disk Confocal) using a 63×/1.4 NA oil immersion objective lens. Seeds were imaged using a 633 nm diode laser, original nanotubes were imaged using a 488 nm diode laser and added monomers were imaged using a 561 nm diode laser. At each imaged location, one image of seeds was captured. Images of the two types of monomers were captured simultaneously in a burst of 20 time-series images using dual cameras.

Replenishment of Medium and Tiles during Time-Lapse Experiments. Tiles for experiments in which the serum-supplemented medium-contained DNA tiles were prepared by annealing 3.6 μM of each of the strands for inactive DNA tiles (Supporting Information S1.3) using the annealing program in *Seed annealing protocol* (Supporting Information SI3.2). Every 12 h, following washing the dish with TAE Mg^{2+} buffer and fluorescence imaging, 50 μL of the annealed inactive DNA tiles was added to the dish sample. Activation strand (10 μM) and 4.2 μM adapter strands were added to the dish sample for desired final concentrations. Two-hundred fifty microliters of 12% FBS-supplemented DMEM medium was added for a total volume of approximately 300 μL. The dish sample was incubated at 37 °C in a temperature-controlled glove box (Coy labs) between imaging, washing, and buffer replacement steps.

Image Processing and Characterization of Nanotube Lengths. Composite two-color images of seeded nanotubes from time-lapse experiments were created by merging two grayscale filter images (Atto647 and Cy3). The same image of the seeds was matched with each of the images of nanotubes to create five images for each location at each time point. To maximize the accuracy of the length determination process, the contrast of each color (seed and nanotube labels) in composite image stacks was enhanced by linear histogram stretching using ImageJ software. Because we could only assess the 2D projection of nanotube length as we imaged the diffusing nanotubes through the bottom of glass dish using epifluorescence, the best estimation of nanotube lengths were made by measuring a nanotube's length in each of the five images captured around a particular time point and selecting the longest of these lengths. The apparent length of a seeded nanotube in a given image was measured by manually drawing segmented lines along the nanotube curves, from the seed to the tip of nanotube, in ImageJ software. Seeded nanotubes whose measured lengths were less than 0.5 μm (about 3 pixels) were counted as having length 0.

Composite images from time-lapse tile incorporation experiments, performed on a spinning disk confocal microscope, were produced likewise by merging the one image of seed (Atto647) with each of the pairs of 20 dual-camera images of nanotubes (Atto488) and added tiles (Cy3) captured at each time point. The contrast of each color channel in composite images was enhanced by linear histogram stretching using ImageJ software. ImageJ's "despeckle" algorithm, which replaced each pixel with the median value in its 3 × 3 neighborhood, was used to further reduce the background noise from free tiles in solution.

Simulation of Nanotube Growth and Repair. Stochastic kinetic simulations of nanotube degradation and repair were performed using the Gillespie algorithm for exact sampling of stochastic kinetic trajectories.[35] Nanotubes were assumed to be six tiles in circumference and the length of the lattice in tiles was converted from the length in tiles assuming each tile row had a size of 14.3 nm.[27,36] Rates of tile degradation and repair were as described in the text. The simulations were implemented in Matlab as a reaction simulator on the cylindrical nanotube lattice that allowed reactions of tile degradation, tile repair at specified rates in units of per tile. Nanotube severing occurred automatically and irreversibly after all of the tiles in a given row were removed. Twenty nanotube degradation trajectories are shown in Figure 4a,d and Figure S12a,d and data from 2000 simulated nanotube degradation processes were simulated to produce the histograms and each curve in Figures 4b,c,e–g and S12b,c,e–g. Simulation code is available upon request.

Atomic Force Microscopy. To characterize PEG-coated seeded nanotubes using atomic force microscopy, 5 μL of sample solution was added to a freshly cleaved mica surface on a puck with a Teflon sheet. A total of 20 μL of 5 mM nickel acetate-supplemented TAE buffer (TAE Ni^{2+} buffer) was then added and the sample was incubated for 5 min to allow the DNA nanostructures to adhere to the surface. The sample on

DOI: 10.1021/acs.nanolett.9b00888
Nano Lett. XXXX, XXX, XXX−XXX

mica was then washed twice with TAE Ni^{2+} buffer. Imaging was performed on a Dimension Icon (Bruker) using Scanasyst mode and sharp nitride lever tip (SNL, 10 C, Bruker) cantilevers. Images were flattened by subtracting a linear function from each scan line using the Nanoscope Analysis software. The lengths and widths of structures were measured using full width at half-maximum of AFM section profile.

■ ASSOCIATED CONTENT

Supporting Information

The SI contains . The Supporting Information is available free of charge on the ACS Publications website at DOI: 10.1021/acs.nanolett.9b00888.

Sequences of DNA molecules used in our experiments, additional experimental results, and simulation results; detailed methods for preparing and anchoring DNA nanostructures (PDF)

Time-lapse fluorescence microscopy showing degradation of seeded DNA nanotubes anchored on a glass coverslip remained intact for hours before rapid disassembly when incubated in serum-supplemented medium at 37 °C (AVI)

■ AUTHOR INFORMATION

Corresponding Author

*E-mail: rschulm3@jhu.edu.

ORCID

Yi Li: 0000-0001-7916-0741

Rebecca Schulman: 0000-0003-4555-3162

Notes

The authors declare no competing financial interest.

■ ACKNOWLEDGMENTS

The authors thank Sisi Jia, Samuel Schaffter, and Joanna Schneider for helpful advice and discussion. This work was supported by DARPA YFA D16AP00147 to R.S.

■ REFERENCES

(1) Seeman, N. C.; Sleiman, H. F. DNA nanotechnology. *Nat. Rev. Mater.* **2017**, *3* (1), 17068.

(2) Rothemund, P. W. Folding DNA to create nanoscale shapes and patterns. *Nature* **2006**, *440* (7082), 297−302.

(3) Douglas, S. M.; Dietz, H.; Leidl, T.; Högberg, B.; Graf, F.; Shih, W. M. Self-assembly of DNA into nanoscale three-dimensional shapes. *Nature* **2009**, *459*, 414−418.

(4) Ke, Y.; Ong, L. L.; Shih, W. M.; Yin, P. Three-Dimensional Structures Self-Assembled from DNA Bricks. *Science* **2012**, *338* (6111), 1177−1183.

(5) Zhang, F.; Jiang, S.; Wu, S.; Li, Y.; Mao, C.; Liu, Y.; Yan, H. Complex wireframe DNA origami nanostructures with multi-arm junction vertices. *Nat. Nanotechnol.* **2015**, *10* (9), 779−784.

(6) Suzuki, Y.; Endo, M.; Sugiyama, H. Lipid-bilayer-assisted two-dimensional self-assembly of DNA origami nanostructures. *Nat. Commun.* **2015**, *6* (1), 9052.

(7) Andersen, E. S.; Dong, M.; Nielsen, M. M.; Jahn, K.; Subramani, R.; Mamdouh, W.; Kjems, J.; et al. Self-assembly of a nanoscale DNA box with a controllable lid. *Nature* **2009**, *459* (7243), 73−76.

(8) Li, J.; Pei, H.; Zhu, B.; Liang, L.; Wei, M.; He, Y.; Fan, C.; et al. Self-Assembled Multivalent DNA Nanostructures for Noninvasive Intracellular Delivery of Immunostimulatory CpG Oligonucleotides. *ACS Nano* **2011**, *5* (11), 8783−8789.

(9) Douglas, S. M.; Bachelet, I.; Church, G. M. A Logic-Gated Nanorobot for Targeted Transport of Molecular Payloads. *Science* **2012**, *335* (6070), 831−834.

(10) Jiang, Q.; Song, C.; Nangreave, J.; Liu, X.; Lin, L.; Qiu, D.; Ding, B.; et al. DNA Origami as a Carrier for Circumvention of Drug Resistance. *J. Am. Chem. Soc.* **2012**, *134* (32), 13396−13403.

(11) Hahn, J.; Wickham, S. F.; Shih, W. M.; Perrault, S. D. Addressing the Instability of DNA Nanostructures in Tissue Culture. *ACS Nano* **2014**, *8* (9), 8765−8775.

(12) Kawane, K.; Motani, K.; Nagata, S. DNA Degradation and Its Defects. *Cold Spring Harbor Perspect. Biol.* **2014**, *6* (6), a016394.

(13) Surana, S.; Bhatia, D.; Krishnan, Y. A method to study in vivo stability of DNA nanostructures. *Methods* **2013**, *64* (1), 94−100.

(14) Mei, Q.; Wei, X.; Su, F.; Liu, Y.; Youngbull, C.; Johnson, R.; Meldrum, D.; et al. Stability of DNA Origami Nanoarrays in Cell Lysate. *Nano Lett.* **2011**, *11* (4), 1477−1482.

(15) Conway, J. W.; Mclaughlin, C. K.; Castor, K. J.; Sleiman, H. DNA nanostructure serum stability: Greater than the sum of its parts. *Chem. Commun.* **2013**, *49* (12), 1172.

(16) Cassinelli, V.; Oberleitner, B.; Sobotta, J.; Nickels, P.; Grossi, G.; Kempter, S.; Manetto, A.; et al. One-Step Formation of "Chain-Armor"-Stabilized DNA Nanostructures. *Angew. Chem., Int. Ed.* **2015**, *54* (27), 7795−7798.

(17) Kiviaho, J. K.; Linko, V.; Ora, A.; Tiainen, T.; Järvihaavisto, E.; Mikkilä, J.; Kostiainen, M. A.; et al. Cationic polymers for DNA origami coating − examining their binding efficiency and tuning the enzymatic reaction rates. *Nanoscale* **2016**, *8* (22), 11674−11680.

(18) Perrault, S. D.; Shih, W. M. Virus-Inspired Membrane Encapsulation of DNA Nanostructures To Achieve In Vivo Stability. *ACS Nano* **2014**, *8* (5), 5132.

(19) Ponnuswamy, N.; Bastings, M. M.; Nathwani, B.; Ryu, J. H.; Chou, L. Y.; Vinther, M.; Shih, W. M.; et al. Oligolysine-based coating protects DNA nanostructures from low-salt denaturation and nuclease degradation. *Nat. Commun.* **2017**, *8*, 15654.

(20) Praetorius, F.; Kick, B.; Behler, K. L.; Honemann, M. N.; Weuster-Botz, D.; Dietz, H. Biotechnological mass production of DNA origami. *Nature* **2017**, *552* (7683), 84−87.

(21) Wang, R.; Zhang, G.; Liu, H. DNA-templated nanofabrication. *Curr. Opin. Colloid Interface Sci.* **2018**, *38*, 88−99.

(22) Lo, P. K.; Metera, K. L.; Sleiman, H. F. Self-assembly of three-dimensional DNA nanostructures and potential biological applications. *Curr. Opin. Chem. Biol.* **2010**, *14* (5), 597−607.

(23) Ko, S.; Liu, H.; Chen, Y.; Mao, C. DNA Nanotubes as Combinatorial Vehicles for Cellular Delivery. *Biomacromolecules* **2008**, *9* (11), 3039−3043.

(24) Stephanopoulos, N.; Freeman, R.; North, H. A.; Sur, S.; Jeong, S. J.; Tantakitti, F.; Stupp, S. I.; et al. Bioactive DNA-Peptide Nanotubes Enhance the Differentiation of Neural Stem Cells Into Neurons. *Nano Lett.* **2015**, *15* (1), 603−609.

(25) Cambridge, S. B.; Gnad, F.; Nguyen, C.; Bermejo, J. L.; Krüger, M.; Mann, M. Systems-wide Proteomic Analysis in Mammalian Cells Reveals Conserved, Functional Protein Turnover. *J. Proteome Res.* **2011**, *10* (12), 5275−5284.

(26) Yen, H. S.; Xu, Q.; Chou, D. M.; Zhao, Z.; Elledge, S. J. Global Protein Stability Profiling in Mammalian Cells. *Science* **2008**, *322* (5903), 918−923.

(27) Mohammed, A. M.; Schulman, R. Directing Self-Assembly of DNA Nanotubes Using Programmable Seeds. *Nano Lett.* **2013**, *13* (9), 4006−4013.

(28) Mohammed, A. M.; Šulc, P.; Zenk, J.; Schulman, R. Self-assembling DNA nanotubes to connect molecular landmarks. *Nat. Nanotechnol.* **2017**, *12* (4), 312−316.

(29) Keum, J.; Bermudez, H. Enhanced resistance of DNA nanostructures to enzymatic digestion. *Chem. Commun.* **2009**, No. 45, 7036.

(30) Rothemund, P. W.; Ekani-Nkodo, A.; Papadakis, N.; Kumar, A.; Fygenson, D. K.; Winfree, E. Design and Characterization of Programmable DNA Nanotubes. *J. Am. Chem. Soc.* **2004**, *126* (50), 16344−16352.

(31) Hariadi, R. F.; Yurke, B.; Winfree, E. Thermodynamics and kinetics of DNA nanotube polymerization from single-filament measurements. *Chem. Sci.* **2015**, *6* (4), 2252−2267.

DOI: 10.1021/acs.nanolett.9b00888
Nano Lett. XXXX, XXX, XXX−XXX

(32) Mardanlou, V.; Yaghoubi, K. C.; Green, L. N.; Subramanian, H. K.; Hariadi, R. F.; Kim, J.; Franco, E. A coarse-grained model captures the temporal evolution of DNA nanotube length distributions. *Nat. Comput.* **2018**, *17* (1), 183−199.
(33) Kielar, C.; Xin, Y.; Shen, B.; Kostiainen, M. A.; Grundmeier, G.; Linko, V.; Keller, A. On the Stability of DNA Origami Nanostructures in Low-Magnesium Buffers. *Angew. Chem.* **2018**, *130* (30), 9614−9618.
(34) Linko, V.; Shen, B.; Tapio, K.; Toppari, J. J.; Kostiainen, M. A.; Tuukkanen, S. One-step large-scale deposition of salt-free DNA origami nanostructures. *Sci. Rep.* **2015**, *5* (1), 15634.
(35) Gillespie, D. T. Exact stochastic simulation of coupled chemical reactions. *J. Phys. Chem.* **1977**, *81* (25), 2340−2361.
(36) Fu, T.; Seeman, N. DNA double-crossover molecules. *Biochemistry* **1993**, *32* (13), 3211−3220.

DOI: 10.1021/acs.nanolett.9b00888
Nano Lett. XXXX, XXX, XXX−XXX